Mechanistic Characterization of Cardiac Arrhythmia from Electrical and Optical Mapping in Langendorff-Perfused Rabbit Hearts

Saleem Ullah, Giovanni V Critelli, Angelica D Quadros, Jimena G S Paredes, Jose C G Junior, Joao Salinet

HEartLab, Federal University of ABC, São Bernardo do Campo, Brazil

Abstract

A comprehensive understanding of the electrophysiological mechanisms driving cardiac arrhythmias is critical for advancing diagnostic and therapeutic approaches. We evaluated simultaneous contact-electrical and panoramic optical mapping in 9 Langendorff-perfused rabbit hearts to compare key biomarkers across rhythms. Arrhythmias were induced with carbachol and an S1–S2 pacing protocol and we recorded atrial and ventricular activity with high-density electrodes and voltage-sensitive dye. We generated isopotential and phase maps, calculated dominant frequency, cycle length, and organization index, and identified activation times with fixed thresholds. During organized rhythms, electrical and optical activation patterns agreed closely. For more complex rhythms such as atrial fibrillation, and ventricular fibrillation, this agreement became less consistent. Applying the Independent Component Analysis improved concordance of atrial activation maps and clarified wavefronts. The results of this study demonstrate that optical signals are susceptible to far-field interference. The data also reveal that the complementary nature of the optical and electrical modalities is dependent on the specific cardiac rhythm. Consequently, these findings underscore the necessity for a more advanced signal processing pipeline for optical mapping to ensure data accuracy.

1. Introduction

Cardiac arrhythmias, or irregular heart rhythms, are a significant global health issue and account for 10–15% of all deaths and substantial healthcare costs [1]. An understanding of the underlying electrophysiological mechanisms, such as enhanced automaticity, triggered activity, and re-entry, is essential for the development of improved diagnostic and therapeutic strategies [2]. Atrial arrhythmias, including atrial fibrillation (AF), often cause poor circulation and increase stroke risk [3]. In contrast, ventricular arrhythmias, such as ventricular tachycardia (VT) and ventricular fibrillation (VF), can lead to sudden cardiac arrest and present immediate life-threatening risks.

New Zealand white rabbits are a key animal model in arrhythmia research because their physiological similarity to humans allows findings from controlled studies to be translated into clinical applications [4]. In this work, we induced arrhythmias in Langendorff-perfused rabbit hearts with carbachol infusion and electrical pacing, and we recorded cardiac activity using simultaneous electrical and optical mapping [5]. This study aims to mechanistically characterize these arrhythmias through a systematic comparison of data from high-density electrical and panoramic optical mapping. This process includes the use of the FastICA algorithm to remove ventricular far-field/scattering artifacts from atrial signals to ensure a more accurate analysis of arrhythmia mechanisms.

2. Methods

Nine New Zealand white rabbits (3.44 ± 0.36 kg) were used for this study under protocol no. 3947230519, approved by the local Committee on Ethics in the Use of Animals (CEUA). As previously reported, animals were anesthetized, euthanized via thoracotomy under deep anesthesia, and their hearts excised and connected to a Langendorff perfusion system [5]. A heated modified Krebs-Henseleit was perfused through the aorta to maintain physiological conditions, with (-)-Blebbistatin used as an uncoupler to suppress mechanical contractions, minimizing motion artifacts during optical mapping.

2.1. Langendorff Heart Perfusion

The hearts were perfused retrogradely at 37°C with a modified Krebs-Henseleit solution buffer at a flow rate of 20–40 mL/min, maintaining a pressure of approximately 80 mmHg. The buffer composition included 118 mM NaCl, 4.7 mM KCl, 1.2 mM $MgSO_4$, 1.2 mM KH_2PO_4, 25 mM $NaHCO_3$, 5.5 mM glucose, 2 mM Na-pyruvate and 2 mM $CaCl_2$, oxygenated with a 95% O_2/5% CO_2 mixture to achieve a pH of 7.4 ± 0.1. Carbachol (1 μM) was infused into the perfusate to induce arrhythmias. Arrhythmias were induced using an S1-S2 epicardial pacing protocol (triple trains of 100 pulses, 20 Hz, 2 ms pulse width, 1.3 s intervals). To ensure optical signal clarity, contractions of were suppressed with (-)-Blebbistatin, administered initially at 20 μM and maintained at 1.7 μM [5].

2.2. Data Acquisition

Electrical mapping utilized a high-density epicardial electrode array (16 electrodes in a 4x4 configuration) positioned on the atria and ventricles, with signals amplified and digitized at 4 kHz using an Open Ephys system equipped with a 64-channel Headstage and acquisition board. For each atrium, a 16-channel electrode array was used. The electrodes were spaced 2 mm apart from each other. The array dimensions were 9.5 mm in width and 14 mm in height. A 16-channel electrode array was also used for the ventricle but the electrode spacing varied. The electrodes were spaced 6 mm apart in one direction and 3 mm apart in another. The overall dimensions of the array were 22 mm in width and 19 mm in height. Optical mapping used the voltage-sensitive dye di-4-ANBDQPQ, excited by six deep-red LEDs (650 nm) with band-pass filters, and included a 9 × 9 μm pixel size, a 1.1° sensor (17.6 mm CMOS), a 25 mm focal length lens, and less than 1% distortion within the region of interest. Fluorescence emissions were captured by three high-speed cameras (500 fps, 1000x1264 pixels, Emergent Technologies) positioned at 120° intervals around the heart, each fitted with long-pass filters (715 nm, Semrock, USA), providing panoramic coverage of cardiac activity.

2.3. Preprocessing

Electrical and optical signals were processed to remove noise and artifacts. For electrical recordings, a 6th-order harmonic notch filter removed 60 Hz powerline interference, and a subsequent Butterworth band-pass filter (0.5 Hz to 250 Hz) eliminated baseline drift and high-frequency noise. For optical signals, a 4th-order Butterworth high-pass filter at 0.5 Hz restored the baseline. A spatiotemporal Gaussian smoothing filter (5x5 spatial kernel, 1x7 temporal kernel) was then applied to reduce noise while preserving signal integrity. Fluorescence intensity changes were used as a surrogate for membrane potential. Here, F_0 denotes the fluorescence of the polarized membrane and F denotes that of the depolarised membrane. The relative change $\Delta F/F_0$ was calculated as $(F - F_0)/F_0$.

2.4. Post-Processing

To post-process the data, we first addressed far-field interference from ventricular activity, a common issue in optical mapping that obscures atrial signals. We applied independent component analysis (ICA) using the FastICA algorithm to remove this noise from both electrical and optical atrial recordings [6]. For the electrical signals, ICA was applied to the multi-channel data from the 16-electrode arrays to remove ventricular components. To create a directly comparable dataset for the optical signals, 16 corresponding channels were generated by averaging the fluorescence data (ΔF/F) from the camera pixels surrounding each physical electrode. This ensured both datasets contained 16 signals. ICA was then applied to these average optical signals to separate and remove ventricular contamination.

Following artifact removal, we used Laplacian interpolation to generate high-density, two-dimensional maps from the sparse 16-point MEA recordings [5]. This method models the epicardial surface as a flat mesh and solves a sparse linear system to estimate electrical values at unrecorded points, which creates a complete electrophysiological map (Figure 1) [5].

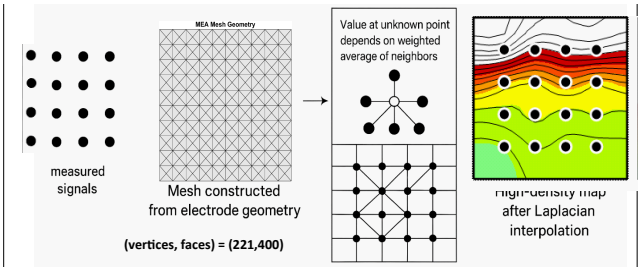

Figure 1: Workflow for generating high-density isopotential maps from sparse electrical recordings.

From this processed data, we analyzed arrhythmia mechanisms by generating isopotential and phase maps. We calculated the dominant frequency (DF) using fourier transform and determined cycle lengths (CL) from the intervals between depolarizations. Additionally, an organization index (OI) was calculated for each optical and electrical signal to quantify its regularity:

$$OI = \frac{\sum(\textbf{Power at DF}) + \sum(\textbf{Power of first 5 DF harmonics})}{\sum(\textbf{Power in the } 2-20 \textbf{ Hz range})}$$

Finally, we visualized wavefront propagation by generating isopotential maps from the interpolated data and creating phase maps with the Hilbert transform [9, 10].

3. Results and Discussion

Our simultaneous electrical and optical mapping revealed that the concordance between the two modalities was highly dependent on rhythm complexity. During organized rhythms such as sinus tachycardia, the propagation agreed closely. As illustrated in Figure 2, except in LA, the activation maps from both techniques showed stable and cohesive wavefront propagation which confirms that the modalities provide comparable results under stable conditions. The LA discrepancy likely reflects residual ventricular far-field contamination that ICA did not fully separate.

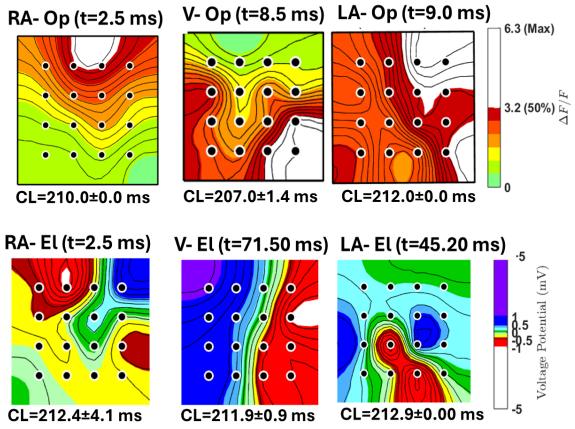

Figure 2. Comparative Analysis of Activation Patterns During Sinus Tachycardia. The figure displays isopotential maps from simultaneous electrical (El) and optical (Op) recordings, showing a concordant activation pattern across the RA, LA, and Ventricle. The measured CL were consistent between optical and electrical recordings, respectively: RA (210.0 ± 0.0 ms vs. 212.4 ± 4.1 ms), Ventricle (207.0 ± 1.4 ms vs. 211.9 ± 0.9 ms), and LA (212.0 ± 0.0 ms vs. 212.9 ± 0.00 ms).

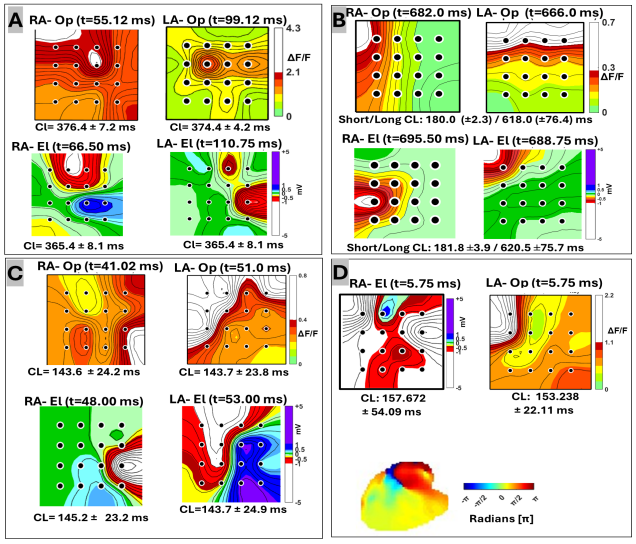

Figure 3. Comparative activation maps for four distinct atrial rhythms: (A) SR, with CLs of RA-OP: 376.4 ± 7.2 ms, RA-El: 365.4 ± 8.1 ms, LA-Op: 374.4 ± 4.2 ms, and LA-El: 365.4 ± 8.1 ms. (B) DA, with dual CLs (OP: 180.0 ± 2.3 ms / 618.0 ± 76.4 ms; El: 181.8 ± 3.9 ms / 620.5 ± 75.7 ms). (C) AT, with CLs of RA-Op: 143.6 ± 24.2 ms, RA-El: 145.2 ± 23.2 ms, LA-Op: 143.7 ± 23.8 ms, and LA-El: 143.7 ± 24.9 ms. (D) AF, with CLs of RA-El: 157.7 ± 54.1 ms and LA-Op: 153.2 ± 22.1 ms. Panel (D) also includes the corresponding optical phase map, which identifies a rotor during AF.

This trend holds for organized atrial arrhythmias. As depicted in Figure 3, rhythms such as sinus rhythm (SR, atrial tachycardia (AT), and a dissociated atria (DA) exhibited consistent and organized propagation patterns when electrical and optical maps were compared (Figure 3A–C). In contrast, activation during AF was highly disorganized Figure 3D. The optical phase map for AF confirmed the presence of a rotor Figure 3D.

A similar divergence is observed in the ventricles, where organized VT produced concordant maps (Figure 4C), while disorganized VF resulted in chaotic and discordant patterns (Figure 4D).

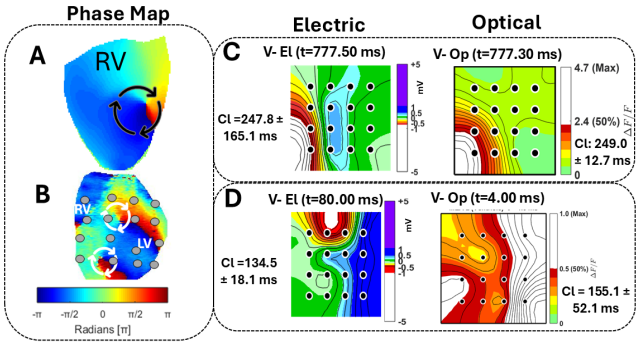

Figure 4. Ventricular arrhythmia mapping. (A) Optical phase map for VT. (B) Optical phase map for VF. (C) Comparative panels for VT: electrical isopotential (left, CL = 247.8± 165.1 ms) and optical fluorescence (right, CL = 249 ± 12.7 ms). (D) Comparative panels for VF: electrical isopotential (left, CL = 134.5 ± 18.1 ms) and optical fluorescence (right, CL = 155.1 ± 52.1 ms).

The DF values were nearly identical during SR. In AF in the LA, the electrically measured mean DF was 6.52 Hz, whereas the optical DF was only 2.98 Hz (Table 1). This disparity could be because contact electrodes are highly sensitive to localized, high-frequency, fractionated signals that are spatially averaged by the panoramic nature of optical mapping. This spatial averaging results in a lower calculated mean DF for the optical data.

The optical recordings of the atria were found to be susceptible to far-field/scattering artifacts from the ventricles, which created misleading activation patterns. The FastICA algorithm effectively removed this interference, and the corrected optical activation maps showed improved concordance with the corresponding electrical maps (Figures 5).

4. Conclusion and Limitations

This research shows that the relationship between panoramic optical and epicardial electrical mapping depends on cardiac rhythm complexity in an ex-vivo rabbit model. The modalities showed high concordance during organized rhythms but provided different, complementary

information during disorganized states like AF and VF. This divergence was clear during AF, where electrical mapping recorded much higher DF than optical mapping. We found that optical signals are susceptible far-field/scattering artifacts from the ventricle and we demonstrated that the FastICA algorithm effectively removes this contamination, which improves the agreement between the two datasets.

Table 1: Comparison of Mean DF and OI between Optical (OP) and Electrical (EL) Mapping

Rhythm	Chamber	Mean OP DF(Hz)	Mean EL DF (Hz)	OP OI	EL OI
SR	RA	2.72	2.80	0.800	0.71
	LA	2.75	2.77	0.804	0.93
ST	RA	4.73	4.67	0.956	0.87
	LA	4.78	4.67	0.940	0.88
	V	4.81	4.41	0.931	0.78
AT	RA	4.64	7.03	0.873	0.87
	LA	6.29	6.00	0.770	0.82
DA	RA	1.27	1.27	0.820	0.82
	LA	1.30	1.10	0.800	0.78
AF	RA	2.40	5.08	0.412	0.33
	LA	2.98	6.52	0.419	0.23
VT	V	8.11	7.85	0.914	0.70
VF	V	5.40	6.40	0.596	0.51

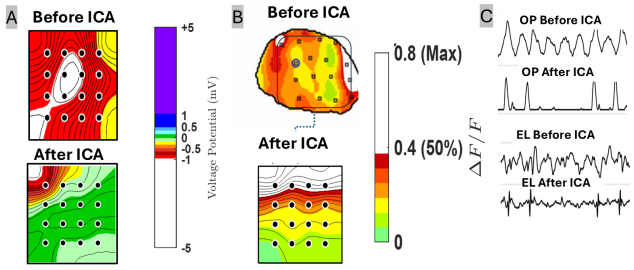

Figure 5. Comparison of simultaneous electrical and optical activation maps. Panels show (A) electrical iso-potential propagation maps, (B) optical propagation maps, and (C) corresponding signal tracings, each presented before (top) and after (bottom) the application of ICA.

Acknowledgments

This study is supported by grant no. 2018/25606-2, São Paulo Research foundation (FAPESP) and CNPq INCT INTERAS. call 58/2022. S. Ullah is supported by Coordenacão de Aperfeiçoamento de Pessoal de Nível Superior – Brasil (CAPES). J. Siles and A. Quadros are supported by grants no. 2020/03601-9 and 2023/06306-6, respectively, FAPESP.

References

[1] D. J. Blackwell *et al.*, "Animal models to study cardiac arrhythmias," *Circ. Res.*, vol. 130, no. 12, pp. 1926–1964, 2022.

[2] G. Tse, "Mechanisms of cardiac arrhythmias," *J. Arrhythmia*, vol. 32, no. 2, pp. 75–81, 2015.

[3] S. Nattel, B. Burstein, and D. Dobrev, "Atrial remodeling and atrial fibrillation," *Circ. Arrhythm. Electrophysiol.*, vol. 1, no. 1, pp. 62–73, 2008.

[4] S. M. Pogwizd and D. M. Bers, "Rabbit models of heart disease," Drug Discov. *Today Dis. Models*, vol. 5, no. 3, pp. 185–193, 2008.

[5] J. Siles et al., "An integrated platform for 2-D and 3-D optical and electrical mapping of arrhythmias in Langendorff-perfused rabbit hearts," *J. Physiol.*, 2025. doi: 10.1113/jp287815.

[6] J. J. Rieta and F. Hornero, "Comparative study of methods for ventricular activity cancellation in atrial electrograms of atrial fibrillation," *Physiol. Meas.*, vol. 28, no. 8, pp. 925–936, 2007.

[7] N. Chattipakorn, I. Banville, R. A. Gray, and R. E. Ideker, "Mechanism of ventricular defibrillation for near-defibrillation threshold shocks," *Circulation*, vol. 104, no. 11, pp. 1313–1319, 2001. doi: 10.1161/hc3601.094295.

[8] E. Lagracie, L. Weynans, and Y. Coudière, "Assessment of a threshold method for computing activation maps from reconstructed transmembrane voltages," *Comput. Cardiol. (CinC)*, vol. 51, p. 029, 2024. doi:10.22489/CinC.2024.029.

[9] J. L. Salinet et al., "Persistent atrial fibrillation hierarchical activation: from highest DF sites to wave fractionation at the boundaries," *CinC*, 2017. doi:10.22489/CinC.2017.194-344.

[10] J. L. Salinet et al., "Drifting rotor prevalence is associated with dominant frequency reduction after persistent atrial fibrillation ablation," *CinC*, 2015, pp. 269–272. doi:10.1109/CIC.2015.7408638

Address for correspondence:
Saleem Ullah
HeartLab - Biomedical Engineering - CECS Federal University of ABC - UFABC Street: Av. Anchieta, Sao Bernardo do Campo - SP, Brazil
E-mail address: saleem.ullah@ufabc.edu.br